Distribution of metal artifacts arising from the exomass in small field-of-view cone beam computed tomography scans

Amanda P. Candemil, DDS, MSc,[a] Benjamin Salmon, DDS, PhD,[b,c] Deborah Queiroz Freitas, DDS, MSc, PhD,[a] Francisco Haiter-Neto, DDS, MSc, PhD,[a] and Matheus Lima Oliveira, DDS, MSc, PhD[a]

Objectives. To evaluate the distribution of metal artifacts from the exomass in small field-of-view (FOV) cone beam computed tomography (CBCT) scans.

Study Design. An image phantom was scanned by using 3 CBCT units. Metal objects were positioned in the exomass, and additional CBCT scans were obtained. Mean gray values were obtained from 16 homogeneous areas and the standard deviation was calculated to quantify gray level inhomogeneity according to distinct zones of the FOV: total area and outer, inner, right, left, and mid-zones. The discrepancy between each zone and the total area was calculated to compare different CBCT units. Mean gray, gray level inhomogeneity, and discrepancy values were separately assessed by using analysis of variance (ANOVA) and Tukey's test ($\alpha = 0.05$).

Results. Overall, the mean gray values were significantly lower in the inner zone, and the gray level inhomogeneity values were significantly higher in the inner and mid-zones irrespective of the presence of metal objects in the exomass. The 3 CBCT units presented significantly different discrepancy values in most conditions.

Conclusions. The distribution of metal artifacts from the exomass follows the inherent gray value dispersion of CBCT images, with greater inhomogeneity in the inner zone of the FOV. This is exacerbated when metal objects are in the exomass. (Oral Surg Oral Med Oral Pathol Oral Radiol 2020;130:116−125)

Cone beam computed tomography (CBCT) is an important diagnostic imaging modality used in the dentomaxillofacial field.[1,2] The CBCT volumetric data set is composed of a matrix of very small cubic units referred to as *voxels,* in which the X-ray attenuation coefficient of the object is calculated. The numerical voxel value (henceforth referred to as "gray value") is subsequently converted into a gray level to display images. Although modern CBCT machines produce high-quality images, the resulting gray values are not capable of following a calibrated scale, mainly because of the relatively low energy parameters, the negative interference of scattered radiation as a result of the conic geometry of the incident beam, and the frequent occurrence of artifacts.[3,4]

It is well accepted that metal objects are a great source of beam hardening−related artifacts on CBCT images.[5] Accordingly, their composition, number, and location may affect CBCT image quality by increasing gray value variability.[6-8] During CBCT scanning, multiple basis images are obtained as the X-ray tube and the digital receptor simultaneously rotate around the object of study. Each basis image registers the remaining energy of the X-ray photons after interacting with many structures along their path,[9] which means that even when a small field of view (FOV) is indicated, the structures located outside the FOV, but between the focal spot and the image receptor of the CBCT unit, also known as *exomass,* cannot be disregarded before image reconstruction.

The presence of metal objects in the exomass decreases CBCT gray values (image darkening) and increases gray level inhomogeneity (image deterioration),[10] and metal artifact reduction algorithms are ineffective in reducing such artifacts.[11] Considering the projection geometry in CBCT, which results in a heterogeneous distribution of artifacts in the FOV,[6,12] it is important to evaluate the spread of the artifacts arising from the exomass across different zones of the FOV. This could mainly indicate whether a specific region of the image can represent the characteristics of this artifact in the entire extension of the FOV. From a clinical point of view, this could be beneficial because it may allow for adaptation of the scanning protocol

Statement of Clinical Relevance

Knowledge of the effects of metal objects in the exomass on the mean gray values and gray level inhomogeneity in small field-of-view cone beam computed tomography scans can help clinicians properly position the object of study in the field of view to minimize image degradation.

[a]Division of Oral Radiology, Department of Oral Diagnosis, Piracicaba Dental School, University of Campinas, Piracicaba (São Paulo), Brazil.
[b]Université de Paris, Orofacial Pathologies, Imaging and Biotherapies EA2496 Lab, Montrouge, France.
[c]Dental Medicine Department, AP-HP, Bretonneau Hospital, Paris, France.
Received for publication Oct 19, 2019; returned for revision Dec 11, 2019; accepted for publication Jan 10, 2020.

2212-4403/$-see front matter
https://doi.org/10.1016/j.oooo.2020.01.002

based on a less affected zone in the FOV when objects, such as dental implants, metal restorations, and orthodontic appliances, are in the exomass. Therefore, this study aimed to evaluate effects of different types, numbers, and locations of metal objects in the exomass on the mean gray values, mean gray level inhomogeneity values, and mean discrepancy values between each zone and the total area in small-FOV CBCT scans.

MATERIALS AND METHODS

Custom-developed imaging phantom

An imaging phantom composed of 16 polypropylene tubes filled with a homogeneous hyperdense solution and surrounded by water was custom-developed, as described by Candemil et al.[10] The phantom was intended to simulate complex X-ray interactions with matter and allow for the evaluation of gray level homogeneity.

CBCT image acquisitions

The imaging phantom was centered on a small FOV of 50 × 50 mm such that all 16 polypropylene tubes were included in the FOV. Ten repeated scans were obtained, with a 10-minute interval between scans, using 3 CBCT units: NewTom Giano (QR, Verona, Italy) with exposure settings of 90 kVp, 3 mA, 9 seconds, and a voxel size of 0.1 mm; CS 9300 (Carestream, Rochester, NY) with exposure settings of 90 kVp, 3.2 mA, 20 seconds, and a voxel size of 0.09 mm; and Picasso Trio (Vatech, Seoul, South Korea) with exposure settings of 90 kVp, 3 mA, 24 seconds, and a voxel size of 0.2 mm. The exposure settings were adjusted to produce images that had the greatest possible similarity in radiodensity of the phantom objects.

Two types of metal objects (titanium implants and cylinders of cobalt−chromium (Co-Cr) alloy, each with dimensions of 15 mm height × 5 mm diameter) in 3 quantities (1, 2, or 3) were placed in turn in the exomass (20 mm away from the periphery of the FOV). Ten additional CBCT scans were obtained for each type and quantity of metal object. This was performed to simulate a clinical situation in which the patient has varying types and numbers of metal objects in the dental arch but outside the FOV. When only 1 object was located in the exomass, it was on the right side of the FOV; for 2 objects, they were placed on opposite sides of the FOV (right and left); and for 3 objects, they were placed on both sides and in the anterior region (Figure 1). Thus, a total of 70 scans for each CBCT unit (10 repeated scans × 2 types of metal objects × 3 quantities of metal objects + 10 scans without any metal object in the exomass) was obtained.

CBCT image analysis

Mean gray values were measured by an oral radiologist with greater than 5 years of experience in CBCT image analysis after selecting circular regions of interest of 8 mm^2 in the center of each of the 16 polypropylene tubes and in the most central axial reconstruction (125 mm above the tip of the tube) by using OsiriX MD software (Pixmeo Sarl, Geneva, Switzerland). The 16 mean gray values were grouped into different combinations to cover multiple zones of the FOV, as follows: total area (control), outer zone, inner zone, right zone, left zone, and mid-zone (Figure 2). For each zone, mean gray values were averaged, and the standard deviation was calculated (henceforth referred to as "gray level inhomogeneity value"). Mean gray values indicated the degree of image darkening, and the standard deviation indicated gray value inhomogeneity.

For direct comparisons among the different CBCT units, the discrepancy between the total area and each zone (henceforth referred to as "zone discrepancy") was calculated for both the mean gray and gray level inhomogeneity values.

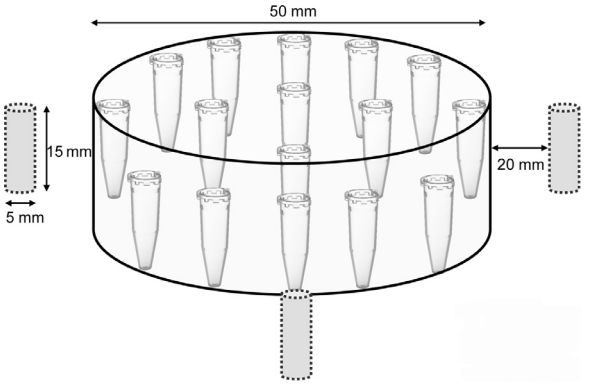

Fig. 1. Schematic drawing illustrating the imaging phantom composed of 16 polypropylene tubes encompassed by the field of view (large solid-line cylinder). The small dotted cylinders represent the locations where the metal objects were placed in the exomass.

Statistical analysis

Prism 8 software (GraphPad, San Diego, CA) was used to perform analysis of variance (ANOVA) and Tukey's test to compare the mean gray and gray level inhomogeneity values among the different FOV zones and to compare the zone discrepancy among the 3 CBCT units for both the mean gray and gray level inhomogeneity values. The significance level was established at 5% ($\alpha = 0.05$).

RESULTS

Total area versus FOV zones

In most of the conditions, compared with the total area, the mean gray values were significantly greater ($P \leq .05$) in the outer, right, and left zones, and significantly lower ($P \leq .05$) in the inner and mid-zones (Table I). Conversely, the values of gray level inhomogeneity were significantly lower ($P \leq .05$) than those in the

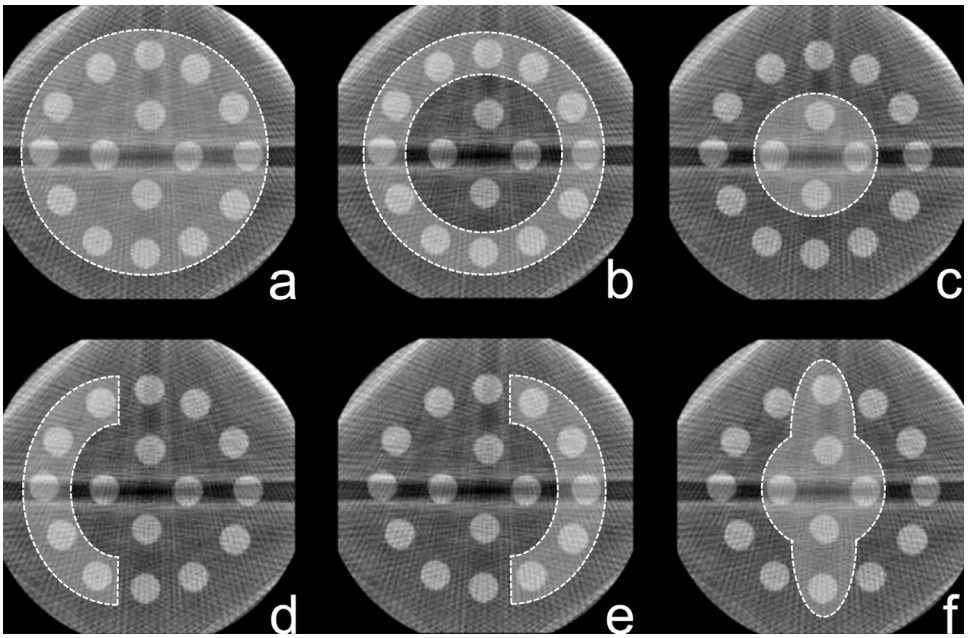

Fig. 2. Representative axial reconstructions of the imaging phantom indicating the different zones of the field of view (FOV) *(shaded area)*. **A,** Total area. **B,** Outer zone. **C,** Inner zone. **D,** Right zone. **E,** Left zone. **F,** Mid-zone.

total area in the outer, right, and left zones, and significantly greater ($P \leq .05$) in the inner and mid-zones, under most of the conditions (Table II).

Inner versus outer versus mid-zones

The inner zone presented significantly lower mean gray values than the mid-zone, which presented significantly lower mean gray values compared with the outer zone ($P \leq .05$), as shown in Table I. In most cases, the outer zone presented the significantly lowest values of gray level inhomogeneity ($P \leq .05$), as shown in Table II.

Right versus left zones

The right zone presented values different from those of the left zone, according to the CBCT unit and the quantity and type of metal objects.

1. *One metal object placed in the exomass (right side of the FOV):* In the NewTom Giano unit, the right zone presented significantly lower mean gray values when the object was a titanium implant, and significantly greater mean gray values when the object was a cylinder of Co-Cr ($P \leq .05$). In the CS 9300 unit, the right zone presented significantly greater mean gray values compared with the left zone ($P \leq .05$) for both types of metal objects. In the Picasso Trio unit, the right zone presented significantly lower mean gray values compared with the left zone ($P \leq .05$) (see Table I). With regard to gray level inhomogeneity, the right zone (adjacent to the object) presented the significantly highest values in all conditions ($P \leq .05$) (see Table II).
2. *Two metal objects placed in the exomass (1 at each side of the FOV):* No significant difference was observed in the mean gray values between the right and left zones for the NewTom Giano and Picasso Trio ($P > .05$) units. However, in the CS 9300 unit, the left zone presented significantly lower mean gray values when the objects were titanium implants and significantly greater mean gray values when the objects were cylinders of Co-Cr ($P \leq .05$) (see Table I). With regard to gray level inhomogeneity, significantly higher values were observed in the left zone in the NewTom Giano unit, and in the right zone in the CS 9300 unit ($P \leq .05$). No significant difference was observed between the gray level inhomogeneity values of the right and left zones in the Picasso Trio unit ($P > .05$) (see Table II).
3. *Three metal objects placed in the exomass (1 at each side of the FOV and the third in the anterior region):* With regard to the mean gray values, the NewTom Giano unit presented no significant difference ($P > .05$) between the right and left zones when the objects were titanium implants; however, in the presence of cylinders of Co-Cr, the right zone presented significantly greater values ($P \leq .05$). Conversely, in the CS 9300 unit, the right zone presented significantly greater values in the presence of titanium implants, and significantly lower values in the presence of cylinders of Co-Cr ($P \leq .05$) (see Table I). With regard to gray level inhomogeneity, in the

Table I. Mean gray values (standard deviation) in function of CBCT unit, object type, quantity, and the field of view zones

CBCT unit	*Object type*	*Quantity*	*Total area*	*Outer zone*	*Inner zone*	*Right zone*	*Left zone*	*Mid-zone*
NewTom Giano	Ti	0	1394.31 (15.67)	1406.47 (15.71)Aa^{ns}	1357.83 (16.37)Ca	1405.13 (14.96)Aa^{ns}	1406.55 (18.46)Aa^{ns}	1375.10 (15.47)Ba
		1	1364.19 (4.81)	1380.03 (4.85)ABb	1316.70 (7.33)Db	1370.26 (5.97)Bb^{ns}	1387.96 (5.49)Ab	1339.34 (6.21)Cb
		2	1311.67 (8.11)	1342.30 (9.07)Ac	1219.78 (7.15)Cc	1339.81 (9.39)Ac	1337.89 (8.43)Ac	1266.38 (8.56)Bc
		3	1280.94 (8.60)	1315.16 (9.90)Ad	1178.27 (7.53)Cd	1324.00 (11.62)Ad	1311.28 (10.24)Ad	1219.77 (7.95)Bd
	Co-Cr	0	1394.31 (15.67)	1406.47 (15.71)Ac^{ns}	1357.83 (16.37)Ca	1405.13 (14.96)Ac^{ns}	1406.55 (18.46)Ac^{ns}	1375.10 (15.47)Bb
		1	1441.81 (4.14)	1469.50 (3.55)Ab	1358.73 (7.96)Da	1475.44 (5.41)Ab	1454.73 (6.14)Bb	1401.46 (5.96)Ca
		2	1326.10 (8.02)	1414.27 (8.46)Ac	1061.59 (7.92)Dc	1395.91 (13.04)Bc	1389.57 (9.87)Bd	1215.03 (7.89)Cd
		3	1423.43 (9.93)	1527.25 (9.90)Aa	1111.99 (12.04)Db	1539.83 (14.66)Aa	1512.15 (9.49)Ba	1252.51 (11.90)Cc
CS 9300	Ti	0	1025.87 (3.02)	1038.39 (2.74)Ba	988.32 (5.07)Da	1059.46 (3.16)Aa	116.02 (5.50)Ca	1006.08 (3.89)Da
		1	987.73 (4.05)	1002.04 (3.80)Ba	944.79 (5.89)Ea	1020.10 (4.58)Aa	983.36 (4.16)Ca^{ns}	964.39 (6.00)Da
		2	950.00 (4.27)	971.68 (4.50)ABb	885.55 (5.16)Db	979.11 (4.11)Ab	964.77 (6.10)Bb	913.97 (4.06)Cb
		3	912.33 (4.42)	942.09 (3.92)Bc	823.03 (7.58)Dc	958.24 (4.41)Ac	935.39 (5.93)Bc	854.85 (6.26)Cc
	Co-Cr	0	1025.87 (3.02)	1038.39 (2.74)Ba	988.32 (5.07)Da	1059.46 (3.16)Aa	1016.02 (5.50)Ca	1006.08 (3.89)Da
		1	973.98 (4.03)	990.05 (4.87)Ba	925.78 (3.61)Ea	1000.97 (5.92)Aa	976.36 (4.48)Ca^{ns}	949.50 (3.16)Da
		2	900.15 (17.62)	931.64 (3.33)Bb	828.15 (12.18)Eb	900.95 (3.05)Cb^{ns}	961.43 (4.46)Ab	863.39 (8.31)Db
		3	851.37 (5.70)	882.39 (5.66)Bc	758.32 (10.89)Ec	862.03 (6.22)Cc	924.73 (7.96)Ac	781.36 (9.62)Dc
Picasso Trio	Ti	0	879.73 (5.61)	908.83 (5.63)ABa	792.42 (6.80)Da	903.01 (6.80)Ba	913.59 (7.19)Aa	832.12 (5.20)Ca
		1	862.43 (4.89)	893.16 (4.24)ABb	770.24 (7.47)Db	884.98 (5.17)Bb	900.52 (4.62)Ab	811.90 (5.86)Cb
		2	822.18 (12.30)	861.28 (12.09)Ac	704.91 (13.38)Cc	859.83 (11.84)Ac	856.89 (12.34)Ac	761.89 (13.36)Bc
		3	814.25 (4.37)	851.18 (4.37)Ac	703.44 (6.78)Cc	859.17 (4.77)Ac	849.19 (5.64)Ac	747.69 (6.24)Bd
	Co-Cr	0	879.73 (5.61)	908.83 (5.63)Aa	792.42 (6.80)Ca	903.01 (6.80)Aa	913.59 (7.19)Aa	832.12 (5.20)Ba
		1	839.92 (7.26)	869.57 (7.82)Bb	750.99 (6.47)Eb	853.47 (7.69)Cb	887.31 (8.20)Ab	789.14 (6.98)Db
		2	772.57 (4.41)	824.25 (3.54)Ac	617.54 (8.67)Cc	819.01 (3.80)Ac	819.09 (3.80)Ac	695.12 (6.42)Bc
		3	727.19 (10.84)	781.12 (9.66)Ad	565.41 (15.19)Cd	785.31 (9.66)Ad	783.12 (8.92)Ad	632.16 (12.98)Bd

Mean values followed by distinct letters (upper case in horizontal and lower case in vertical, for each object and CBCT unit) differ significantly from each other ($P \leq .05$).
CBCT, cone beam computed tomography; *Co-Cr,* cobalt−chromium; *ns,* not significantly different from the control group; *Ti,* titanium.

Table II. Mean values (standard deviation) of gray level inhomogeneity in function of CBCT unit, object type, quantity, and the field of view zones

CBCT unit	*Object type*	*Quantity*	*Total area*	*Outer zone*	*Inner zone*	*Right zone*	*Left zone*	*Mid-zone*
NewTom Giano	Ti	0	24.21 (3.07)	10.65 (3.47)Bb	10.03 (4.78)Bd	9.52 (3.81)Bb	10.11 (5.84)Bb	28.51 (3.77)Ad^{ns}
		1	33.48 (2.65)	16.09 (3.56)BCb	24.46 (4.68)Bc^{ns}	17.44 (5.17)BCb	11.88 (3.69)Cb	40.24 (3.80)Ac^{ns}
		2	92.67 (3.12)	61.56 (4.17)Ca	118.11 (5.35)Aa	58.84 (5.12)Ca	81.91 (6.28)Ba	116.68 (4.26)Aa
		3	95.70 (3.15)	68.52 (3.74)Ca	98.73 (5.56)ABb^{ns}	66.62 (11.29)Ca	88.78 (4.66)Ba^{ns}	100.92 (4.57)Ab^{ns}
	Co-Cr	0	24.21 (3.07)	10.65 (3.47)Bc	10.03 (4.78)Bd	9.52 (3.81)Bc	10.11 (5.84)Bc	28.51 (3.77)Ad^{ns}
		1	66.85 (4.47)	42.31 (4.83)Cb	58.83 (5.12)Bc^{ns}	56.32 (13.25)Bb	27.13 (5.27)Db	80.52 (4.95)Ac
		2	345.90 (9.77)	268.95 (11.10)Ea	461.64 (10.10)Aa	300.90 (18.39)Da	321.96 (8.94)Ca	429.46 (7.87)Ba
		3	341.26 (5.76)	263.44 (10.37)Ea	393.80 (8.43)Ab	293.59 (25.60)Da	321.61 (6.19)Ca	366.69 (5.89)Bb
CS 9300	Ti	0	39.41 (1.36)	37.10 (1.71)Ac^{ns}	13.65 (2.93)Cc	29.60 (2.98)Bc	24.68 (3.29)Bc	41.65 (2.40)Ac^{ns}
		1	46.58 (1.58)	40.00 (1.20)Bc^{ns}	40.82 (5.58)Bb^{ns}	43.59 (2.90)ABb^{ns}	26.92 (3.28)Cc	51.42 (3.64)Ab^{ns}
		2	80.94 (3.61)	62.62 (2.01)Cb	104.08 (8.72)Aa	90.30 (4.55)Ba	38.66 (4.00)Db	96.58 (7.00)Aba
		3	94.36 (3.11)	73.81 (2.67)Ba	101.55 (7.33)Aa	96.29 (4.03)Aa^{ns}	66.91 (4.37)Ba	95.12 (5.56)Aa^{ns}
	Co-Cr	0	39.41 (1.36)	37.10 (1.71)Ac^{ns}	13.65 (2.93)Cd	29.60 (2.98)Bd	24.68 (3.29)Bc	41.65 (2.40)Ad^{ns}
		1	59.21 (2.51)	48.47 (2.45)Cb	68.90 (5.27)Abc	63.74 (3.82)Bc^{ns}	28.76 (4.14)Dc	71.55 (3.90)Ac
		2	158.82 (5.74)	142.50 (3.35)Da	201.65 (16.89)Ba	224.33 (5.61)Ab	40.97 (5.20)Eb	169.22 (13.01)Ca
		3	158.60 (4.97)	149.19 (3.81)Ca	169.06 (12.51)Bb	232.72 (5.65)Aa	50.11 (5.88)Ea	136.31 (9.77)Db
Picasso Trio	Ti	0	52.99 (1.98)	10.74 (1.41)Bd	7.25 (2.20)Bd	8.33 (2.16)Bd	11.14 (2.29)Bc	61.84 (3.77)Ad
		1	58.46 (1.92)	17.72 (2.08)Cc	28.30 (3.16)Bc	23.97 (3.32)Bc	9.95 (2.72)Dc	68.32 (2.81)Ac
		2	93.99 (2.16)	54.07 (3.05)Da	94.68 (3.86)Ba^{ns}	63.26 (4.16)Ca	61.83 (3.39)Ca	115.00 (2.49)Aa
		3	84.21 (2.32)	48.29 (2.85)Db	70.99 (3.40)Bb	51.68 (5.20)CDb	55.97 (4.34)Cb	89.57 (1.54)Ab
	Co-Cr	0	52.99 (1.98)	10.74 (1.41)Bd	7.25 (2.20)Bd	8.33 (2.16)Bd	11.14 (2.29)Bb	61.84 (3.77)Ad
		1	61.53 (2.34)	28.14 (2.59)Dc	44.09 (3.32)Bc	35.61 (4.28)Cc	12.14 (3.07)Eb	68.40 (1.90)Ac
		2	159.81 (2.39)	110.75 (1.50)Cb	199.83 (5.72)Aa	126.94 (3.96)Bb	130.99 (2.94)Ba	196.06 (3.67)Aa
		3	157.83 (2.75)	117.00 (4.63)Ca	166.49 (5.96)Ab	136.17 (6.28)Ba	133.31 (4.54)Ba	168.18 (3.70)Ab

Mean values followed by distinct letters (upper case in horizontal and lower case in vertical, for each object and CBCT unit) differ significantly from each other ($P \leq .05$).
CBCT, cone beam computed tomography; *Co-Cr,* cobalt−chromium; *ns,* not significantly different from the control group; *Ti,* titanium.

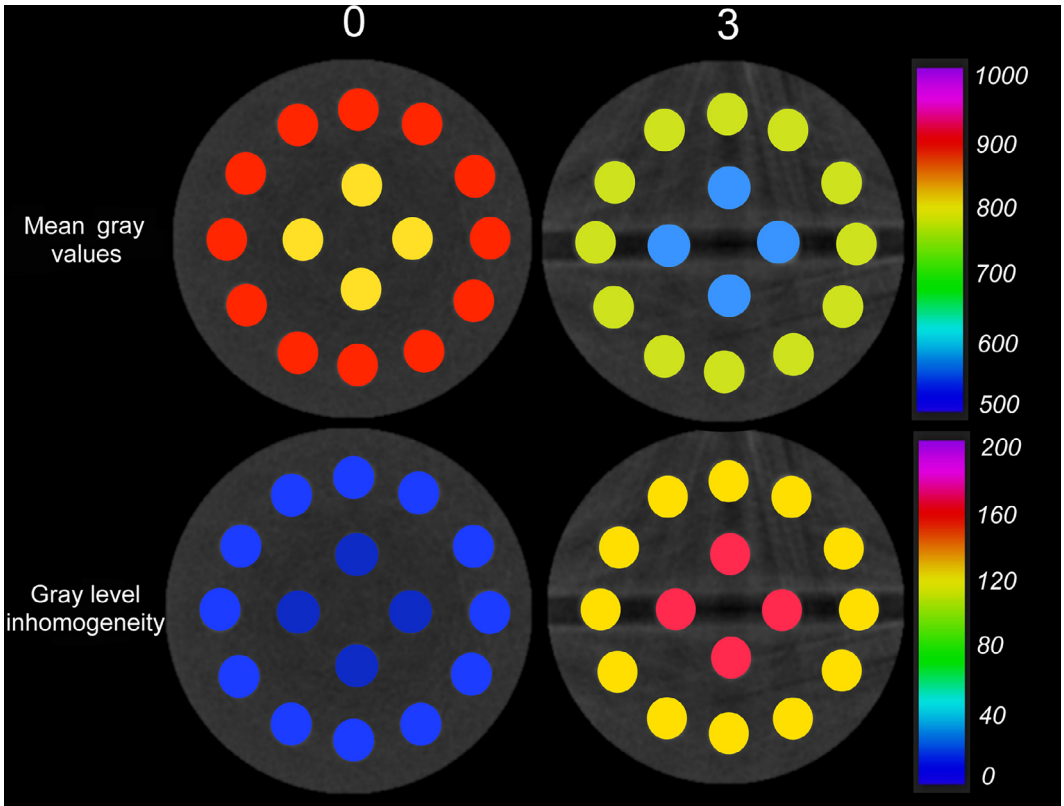

	Quantity	Total area	Outer zone	Inner zone	Right zone	Left zone	Mid zone
Mean gray values	0	879.73	908.83	792.42	903.01	913.59	832.12
	3	727.19	781.12	565.41	785.31	783.12	632.16
Gray level inhomogeneity	0	52.99	10.74	7.25	8.33	11.14	61.84
	3	157.83	117.00	166.49	136.17	133.31	168.18

Fig. 3. Representative color mapping of the mean gray values and gray level inhomogeneity values from axial reconstructions of the imaging phantom without (0) and with 3 cobalt−chromium (Co-Cr) inserts in the exomass (3) obtained with the Picasso Trio unit.

NewTom Giano unit, both types of metal objects presented significantly greater values in the left zone ($P \leq .05$), which is the opposite of the findings in the CS 9300 unit, with the right zone presenting significantly higher values ($P \leq .05$). In the Picasso Trio unit, both the mean gray values and gray level inhomogeneity values did not differ significantly between the right and left zones for either type of metal objects ($P > .05$) (see Tables I and II).

Absence versus presence of metal objects in the exomass

Most conditions with metal objects in the exomass followed the same gray value distribution of the scans without any metal object in the exomass. With regard to the values of gray level inhomogeneity, the outer, right, and left zones followed the same distribution as the scans without any metal object in the exomass, whereas the inner zone presented a significant reduction in relation to the total area ($P \leq .05$), which is the opposite of what occurs in most conditions when metal objects are in the exomass. Figure 3 exhibits the overall outcomes of the mean gray values and gray level inhomogeneity values of representative images obtained with the Picasso Trio unit with and without 3 Co-Cr inserts in the exomass.

Zone discrepancy among the CBCT devices

Under most conditions, the CS 9300 unit showed significantly lower zone discrepancy values for both mean gray values and gray level inhomogeneity values ($P \leq .05$), and the Picasso Trio unit presented significantly higher zone discrepancy for gray level inhomogeneity values ($P \leq .05$) (Tables III and IV).

DISCUSSION

Metal artifacts arising from the exomass have been demonstrated to negatively affect CBCT gray values[10]; however, little is known about the distribution of such image degradation across the FOV. The present investigation generally showed that the mean gray values were increased (brighter image) in the periphery of the FOV (outer, right, and left

Table III. Mean discrepancy values (standard deviation) between the mean gray values of the total area and each individual zone

Zone	*Object type*	*Quantity*	*NewTom Giano*	*CS 9300*	*Picasso Trio*
Outer zone		0	−12.16 (1.48)*	−12.52 (1.00)*	−29.10 (1.14)†
	Ti	1	15.83 (1.63)*	14.31 (1.02)*	30.73 (1.09)†
		2	30.63 (1.71)	21.69 (1.64)*	39.09 (1.02)†
		3	34.22 (2.14)†	29.77 (1.45)*	36.94 (1.38)†
	Co-Cr	1	27.69 (1.65)†	16.07 (1.27)*	29.64 (1.08)†
		2	88.17 (1.30)†	31.49 (15.98)*	51.68 (1.70)
		3	103.81 (1.93)†	31.02 (2.66)*	53.93 (1.84)
Inner zone		0	36.48 (4.43)*	37.56 (2.99)*	87.31 (3.43)†
	Ti	1	−47.50 (4.89)*	−42.94 (3.06)*	−92.19 (3.25)†
		2	−91.89 (5.12)	−64.45 (4.24)*	−117.27 (3.06)†
		3	−102.67 (6.42)	−89.30 (4.35)*	−110.81 (4.13)†
	Co-Cr	1	−83.08 (4.94)†	−48.20 (3.81)*	−88.93 (3.24)†
		2	−264.51 (3.91)†	−72.00 (23.87)*	−155.04 (5.11)
		3	−311.45 (5.79)†	−93.05 (7.97)*	−161.78 (5.52)
Right zone		0	−10.82 (5.28)*	−33.59 (3.48)†	−23.27 (4.17)
	Ti	1	6.06 (4.33)*	32.37 (3.17)†	22.55 (1.64)
		2	28.14 (2.11)*	29.11 (2.27)*	37.64 (3.13)†
		3	43.07 (5.69)*	45.92 (4.14)*	44.92 (3.94)*
	Co-Cr	1	33.63 (7.78)†	26.99 (2.51)	13.55 (2.40)*
		2	69.81 (8.21)†	0.80 (16.34)*	46.43 (2.85)
		3	116.40 (9.29)†	10.66 (4.70)*	58.11 (2.65)
Left zone		0	−12.24 (5.19)	9.85 (3.77)*	−33.85 (2.70)†
	Ti	1	23.77 (2.91)	−4.37 (2.72)*	38.09 (2.21)†
		2	26.21 (4.09)	14.77 (3.63)*	34.71 (1.72)†
		3	30.34 (4.82)†	23.06 (3.71)*	34.95 (3.08)†
	CoCr	1	12.92 (3.16)	2.38 (1.90)*	47.39 (1.92)†
		2	63.50 (5.29)†	61.29 (16.61)	46.52 (2.61)*
		3	88.71 (6.47)†	73.36 (6.40)	55.93 (2.09)*
Mid-zone		0	19.21 (3.06)*	19.79 (1.55)*	47.61 (2.08)†
	Ti	1	−24.86 (3.02)*	−23.34 (3.10)*	−50.53 (2.11)†
		2	−45.20 (3.62)	−36.03 (2.84)*	−60.29 (2.86)†
		3	−61.17 (4.41)*,†	−57.48 (2.60)*	−66.56 (3.56)†
	CoCr	1	−40.34 (3.08)	−24.48 (2.11)*	−50.79 (2.33)†
		2	−111.07 (5.84)†	−36.75 (20.26)*	−77.46 (2.94)
		3	−170.93 (5.11)†	−70.01 (6.20)*	−95.03 (2.93)

*Significantly lower than those in the same row.
†Significantly greater than those in the same row.
Co-Cr, cobalt−chromium; *Ti,* titanium.

zones) and decreased (darker image) in the central region of the FOV (inner and mid zones), in agreement with a previous study,[13] regardless of the presence of metal objects in the exomass. Also, in most cases, the number of metal objects in the exomass was inversely proportional to the mean gray values and directly proportional to the gray level inhomogeneity values, which means that greater numbers of such objects lead to an overall darker and more deteriorated image. We believe this is probably caused by the predominance of hypodense artifacts over hyperdense artifacts, heterogeneously distributed. Previous studies demonstrated that a higher number of metal objects in the FOV leads to a decrease in mean gray values, increase in noise[6,14,15] and gray level inhomogeneity[16]; however, the exomass was not considered in these studies.

In recent years, research has focused on the understanding of the characteristics of CBCT artifacts. Although earlier studies revealed modulating factors in the distribution of artifacts in the image, such as the composition and location of artifact-source objects in the FOV, and the CBCT acquisition parameters,[7,8,17-19] little consideration has been given to artifacts arising from the exomass. Indeed, when using small FOVs, clinicians must be aware that the size of the exomass increases, which may negatively affect image quality, depending on the presence, location, and quantity of radiodense objects (e.g., metals) in the exomass.

Artifacts are not produced homogeneously on the CBCT image,[4] which was confirmed in the present research. Other studies revealed reduced overall image noise when the source of the artifact was placed in the center of the FOV rather than in the periphery.[20,21] Another study using titanium or zirconium dental implants reported greater image noise in the vicinity of the source of the artifact.[17] Although our investigation also observed inhomogeneity of the gray values in the FOV and greater

Table IV. Mean discrepancy values (standard deviation) between the values of gray level inhomogeneity of the total area and each individual zone

Zone	*Object type*	*Quantity*	*NewTom Giano*	*CS 9300*	*Picasso Trio*
Outer zone		0	13.56 (2.56)	2.31 (1.18)*	42.25 (2.71)†
	Ti	1	−17.38 (3.82)	−6.58 (1.40)*	−40.74 (2.44)†
		2	−31.11 (3.71)	−18.32 (3.15)*	−39.92 (2.33)†
		3	−27.18 (3.91)	−20.55 (2.37)*	−35.92 (2.58)†
	Co-Cr	1	−24.54 (2.48)	−10.75 (1.77)*	−33.40 (1.67)†
		2	−76.95 (6.93)†	−16.32 (5.77)*	−49.05 (1.37)
		3	−77.83 (5.79)†	−9.41 (3.93)*	−40.84 (2.92)
Inner zone		0	14.18 (5.85)*	25.76 (3.23)	45.74 (2.23)†
	Ti	1	−9.02 (4.69)*	−5.76 (5.00)*	−30.15 (3.01)†
		2	25.45 (3.90)†	23.14 (5.43)†	0.69 (2.40)*
		3	3.02 (4.71)*	7.18 (5.24)*	−13.22 (3.80)†
	Co-Cr	1	−8.02 (5.30)*	9.69 (3.93)	−17.45 (3.70)†
		2	115.75 (8.79)†	42.83 (1194)*	40.02 (5.34)*
		3	52.54 (8.91)†	10.46 (8.76)*	8.66 (4.41)*
Right zone		0	14.69 (4.11)	9.80 (2.82)*	44.66 (2.78)†
	Ti	1	−16.04 (4.42)	2.99 (3.22)*	−34.48 (3.56)†
		2	−33.83 (4.86)†	9.36 (4.11)*	−30.73 (2.92)†
		3	−29.08 (11.08)†	1.93 (2.29)*	−32.54 (5.02)†
	Co-Cr	1	−10.53 (11.56)	4.53 (3.11)*	−25.92 (2.65)†
		2	−44.99 (17.29)	65.51 (6.26)†	−32.87 (3.69)*
		3	−47.68 (21.06)	74.13 (5.06)†	−21.66 (4.36)*
Left zone		0	14.11 (4.35)*	14.72 (3.44)*	41.85 (2.66)†
	Ti	1	−21.59 (4.84)*	−19.66 (3.88)*	−48.51 (3.25)†
		2	−10.76 (5.56)*	−42.28 (4.99)†	−32.15 (3.00)
		3	−6.92 (5.21)*	−27.45 (4.84)†	−28.25 (4.23)†
	Co-Cr	1	−39.72 (3.84)	−30.46 (4.81)*	−49.39 (2.67)†
		2	−23.93 (10.87)*	−117.85 (6.96)	−28.82 (2.75)*
		3	−19.65 (6.90)*	−108.49 (7.16)	−24.52 (2.64)*
Mid-zone		0	−4.30 (2.13)*	−2.25 (2.31)*	−8.85 (2.47)†
	Ti	1	6.77 (1.94)*,†	4.84 (3.09)*	9.86 (1.51)†
		2	24.01 (2.02)†	15.64 (3.99)*	21.01 (1.31)†
		3	5.22 (3.22)†	0.75 (3.27)*	5.35 (2.42)†
	Co-Cr	1	13.67 (3.56)†	12.34 (1.88)†	6.87 (1.19)*
		2	83.56 (7.25)†	10.40 (8.17)*	36.25 (2.27)
		3	33.73 (6.13)†	−22.29 (6.31)	10.35 (1.89)*

*Significantly lower than those in the same row.
†Significantly greater than those in the same row.
Co-Cr, cobalt−chromium; *Ti,* titanium.

values of gray level inhomogeneity in the central region, the artifacts produced came from the exomass.

In this study, both the inner and mid-zones presented a significant reduction of mean gray values; however, when comparing the values of gray level inhomogeneity among the FOV zones, in most cases, the mid-zone presented significantly greater values. This may be explained by the fact that the mid-zone differs from the inner zone in that the former incorporates 2 regions of the outer zone, which presents significantly different values and increases the standard deviation (gray level inhomogeneity values) within the mid-zone.

Different CBCT units presented different behaviors between the right and left zones in this study. This could reflect some peculiarities of image reconstruction and scanning parameters. For instance, the rotation arc and number of basis images are, respectively, 360 degrees and 360 for the NewTom Giano unit; 180+7 degrees and 480 for the CS 9300 unit; and 360 degrees and 720 for the Picasso Trio unit. When comparing zone discrepancy for both mean gray values and gray level inhomogeneity values among the CBCT units used, the CS 9300 unit presented images with the lowest values, and this reveals a more homogeneous distribution of the metal artifacts from the exomass across the FOV. This may possibly be explained by a machine-specific reconstruction process and/or the unavoidable minimum difference in the X-ray exposure settings between the NewTom Giano (3 mA, 9 seconds, voxel size of 0.1 mm); CS 9300 (3.2 mA, 20 seconds, voxel size of 0.09 mm); and Picasso Trio (3 mA, 24 seconds, voxel size of 0.2 mm) units. Although the CBCT energy parameters were not investigated as independent variables in the present research, theoretical background supports the hypothesis that increased milliamperage and

kilovoltage would increase the signal-to-noise ratio and possibly reduce beam hardening–related artifacts. However, a previous study assessing the variability of CBCT voxel values when artifacts are induced from objects in the FOV revealed that milliamperage did not affect image homogeneity.[22]

When translating the outcomes of the present study to clinical practice, some CBCT image deterioration may be expected when small FOVs are indicated for patients presenting objects of high density and atomic number in the oral cavity. Contemporary oral rehabilitation procedures employ diverse dental materials, such as titanium and zirconium implants, metallic pins, and zirconium crowns, that make this a daily-encountered condition. Conversely, CBCT scans with larger FOV sizes present less image noise,[6,14,23,24] probably as a result of the relative reduction of the exomass. However, they undoubtedly deliver a higher x-radiation dose to the patient, which might be acceptable if the final image quality allows for improved diagnostic accuracy. This is a key point in the principle of optimization of radiographic exposures by adhering to the ALADAIP principle (keeping radiographic exposure As Low As Diagnostically Acceptable being Indication-oriented and Patient-specific).[25]

In our study, the artifacts arising from the exomass showed different characteristics compared with artifacts arising from objects present in the FOV.[17] When a CBCT examination is indicated, it is important that the clinician evaluate possible artifact sources and their locations regarding the structure of interest. Thus, by balancing the radiation dose factor, a suitable FOV size that results in less image quality damage can be selected. Despite the statistically significant differences observed in this *in vitro* study, future research is recommended to investigate the clinical relevance in many diagnostic tasks and the possible interference of exposure factors under optimized conditions.

CONCLUSIONS

The distribution of metal artifacts arising from the exomass on a small field-of-view CBCT scan follows the inherent gray value dispersion. However, the presence of metal objects in the exomass exacerbates image inhomogeneity in the central region of the FOV and among different zones of the FOV. Therefore, professionals are advised to avoid placing the object of study in the center of the FOV when metallic objects are in the exomass.

FUNDING

We gratefully acknowledge the financial support from Coordenação de Aperfeiçoamento de Pessoal de Nível Superior – Brazil (CAPES) (finance code 001) and from the International Relations Office (DERI; 26/2016) at UNICAMP.

REFERENCES

1. Abramovitch K, Rice DD. Basic principles of cone beam computed tomography. *Dent Clin North Am*. 2014;58:463-484.
2. Scarfe W, Farman A. What is cone-beam CT, and how does it work? *Dent Clin North Am*. 2008;52:707-730.
3. Molteni R. Prospects and challenges of rendering tissue density in Hounsfield units for cone beam computed tomography. *Oral Surg Oral Med Oral Pathol Oral Radiol*. 2013;116:105-119.
4. Parsa A, Ibrahim N, Hassan B, Van der Stelt P, Wismeijer D. Influence of object location in cone beam computed tomography (NewTom 5 G and 3 D Accuitomo 170) on gray value measurements at an implant site. *Oral Radiol*. 2014;30:153-159.
5. Chang E, Lam E, Shah P, Azarpazhooh A. Cone-beam computed tomography for detecting vertical root fractures in endodontically treated teeth: a systematic review. *J Endod*. 2016;42:177-185.
6. Pauwels R, Jacobs R, Bogaerts R, Bosmans H, Panmekiate S. Reduction of scatter-induced image noise in cone beam computed tomography: effect of field of view size and position. *Oral Surg Oral Med Oral Pathol Oral Radiol Endod*. 2016;121:188-195.
7. Lagravère MO, Carey J, Ben-Zvi M, Packota GV, Major PW. Effect of object location on the density measurement and Hounsfield conversion in a NewTom 3 G cone beam computed tomography unit. *Dentomaxillofac Radiol*. 2008;37:305-308.
8. Nackaerts O, Maes F, Yan H, Couto Souza P, Pauwels R, Jacobs R. Analysis of intensity variability in multislice and cone beam computed tomography. *Clin Oral Implants Res*. 2011;22:873-879.
9. Farman AG, Scarfe WC. The basics of maxillofacial cone beam computed tomography. *Semin Orthod*. 2009;15:2-13.
10. Candemil AP, Salmon B, Freitas DQ, Ambrosano GM, Haiter-Neto F, Oliveira ML. Metallic materials in the exomass impair cone beam CT voxel values. *Dentomaxillofac Radiol*. 2018;27:20180011.
11. Candemil AP, Salmon B, Freitas DQ, Ambrosano GMB, Haiter-Neto F, Oliveira ML. Are metal artefact reduction algorithms effective to correct cone beam CT artefacts arising from the exomass? *Dentomaxillofac Radiol*. 2019;48:20180290.
12. Bechara BB, Moore WS, McMahan CA, Noujeim M. Metal artefact reduction with cone beam CT: an in vitro study. *Dentomaxillofac Radiol*. 2012;41:248-253.
13. Bryant J A, Drage N A, Richmond S. Study of the scan uniformity from an i-CAT cone beam computed tomography dental imaging system. *Dentomaxillofac Radiol*. 2008;37:365-374.
14. Katsumata A, Hirukawa A, Okumura S, et al. Relationship between density variability and imaging volume size in cone-beam computerized tomographic scanning of the maxillofacial region: an in vitro study. *Oral Surg Oral Med Oral Pathol Oral Radiol Endod*. 2009;107:420-425.
15. Nishikawa K, Kousuge Y, Sano T. Is application of a quantitative CT technique helpful for quantitative measurement of bone density using dental cone-beam CT? *Oral Radiol*. 2016;32:9-13.
16. Oliveira ML, Tosoni GM, Lindsey DH, Mendonza K, Tetradis S, Mallya SM. Assessment of CT numbers in limited and medium field-of-view scans taken using Accuitomo 170 and Veraviewepocs 3 De cone-beam computed tomography scanners. *Imaging Sci Dent*. 2014;44:279-285.
17. Fontenele RC, Nascimento EH, Vasconcelos TV, Noujeim M, Freitas DQ. Magnitude of cone beam CT image artifacts related to zirconium and titanium implants: impact on image quality. *Dentomaxillofac Radiol*. 2018;10:20180021.
18. Freitas DQ, Fontenele RC, Nascimento EHL, Vasconcelos TV, Noujeim M. Influence of acquisition parameters on the magnitude of cone beam computed tomography artifacts. *Dentomaxillofac Radiol*. 2018;47:20180151.
19. Kuusisto N, Huumonen S, Kotiaho A, Haapea M, Rekola J, Vallittu P. Intensity of artefacts in cone beam CT examinations

caused by titanium and glass fibre-reinforced composite implants. *Dentomaxillofac Radiol*. 2019;48:20170471.
20. Taylor C. Evaluation of the effects of positioning and configuration on contrast-to-noise ratio in the quality control of a 3 D Accuitomo 170 dental CBCT system. *Dentomaxillofac Radiol*. 2016;45:20150430.
21. Queiroz PM, Santaella GM, da Paz TD, Freitas DQ. Evaluation of a metal artefact reduction tool on different positions of a metal object in the FOV. *Dentomaxillofac Radiol*. 2017;46:20160366.
22. Oliveira ML, Freitas DQ, Ambrosano GM, Haiter-Neto F. Influence of exposure factors on the variability of CBCT voxel values: a phantom study. *Dentomaxillofac Radiol*. 2014;43:20140128. Erratum in: *Dentomaxillofac Radiol*. 2014;43:20149002.
23. Pauwels R, Stamatakis H, Bosmans H, et al. Quantification of metal artefacts on cone beam computed tomography images. *Clin Oral Implants Res*. 2013;24:94-99.
24. Nardi C, Borri C, Regini F, et al. Metal and motion artefacts by cone beam computed tomography (CBCT) in dental and maxillofacial study. *Radiol Med*. 2015;120:618-626.
25. Oenning AC, Jacobs R, Pauwels R, et al. Cone-beam CT in paediatric dentistry: DIMITRA project position statement. *Pediatr Radiol*. 2018;48:308-316.

Reprint requests:

Amanda P. Candemil
Department of Oral Diagnosis
Piracicaba Dental School
University of Campinas
Av. Limeira, 901, Piracicaba
São Paulo 13414-903
Brazil.
amandacandemil@hotmail.com